Case Studies in Construction Materials 16 (2022) e00906

Contents lists available at ScienceDirect

Case Studies in Construction Materials

journal homepage: www.elsevier.com/locate/cscm

Low-grade RC beams strengthened with TRM composite based on basalt, carbon and steel textiles: Experimental and analytical study

Pello Larrinaga [a], Leire Garmendia [b], Carlos Chastre [c], José-Tomás San-José [d,*]

[a] ENEDI research group, Energy Engineering Department, Engineering Faculty of Bilbao, University of the Basque Country - UPV/EHU. Plaza Torres Quevedo 1, 48013 Bilbao, Spain
[b] Department of Mechanical Engineering, Engineering Faculty of Bilbao, University of the Basque Country - UPV/EHU. Plaza Torres Quevedo 1, 48013 Bilbao, Spain
[c] CERIS and Department of Civil Engineering, NOVA School of Science and Technology, 2829-516 Caparica, Portugal
[d] Department of Mining, Metallurgical and Mat, Science, Engineering Faculty of Bilbao, University of the Basque Country - UPV/EHU. Plaza Torres Quevedo 1, 48013 Bilbao, Spain

ARTICLE INFO

Keywords:
Composite
Concrete
Flexural strengthening
Numerical approach
Textile

ABSTRACT

This study develops an easy-to-conduct numerical calculation method to assess the effect of Textile Reinforced Mortar when used as externally bonded flexural strengthening technique in low-grade reinforced concrete beams from ancient structures (aged between 60 and 100 years old). Using materials main mechanical characteristics and the beams dimensions as inputs, the model defines the behaviour of the strengthened elements. This paper includes the experimental characterization of the whole strengthening solution, from the constituent materials and the composite in pure tensile to scaled beams strengthened in flexure. In total three different materials – basalt, carbon and steel cords – are used as Textile Reinforced Mortar inner reinforcement. Tests are carried out on sixteen low-grade reinforced concrete beams that reproduce low-quality concretes with a compression strength below 17 MPa and, in general, poor mechanical properties, as those present in old and decayed structures. This experimental campaign includes the study of two other particular features of the adopted retrofitting technique: the strengthening ratio and the use of an anchorage system.

The obtained experimental findings are assessed and satisfactorily compared with the developed numerical approach, leading us to conclude that Textile Reinforced Mortar is an effective solution for retrofitting structures made of low-grade reinforced concretes in terms of increasing their deformation and load-bearing capacity under flexural loads (the maximum bending moment has increased between 30% and 200%). Besides, the failure mechanism due to undesired premature detachment was effectively countered using U-shaped anchors, failing the strengthened beams due to the composite tensile failure.

1. Introduction

The profound financial and social crisis of the decade leading up to 2010 gravely affected the macro sector of Construction in Spain, which despite all obstacles, continues to make a considerable contribution to Gross Domestic Product (GDP), which stood at 5.6% in

* Corresponding author.
E-mail address: josetomas.sanjose@ehu.es (J.-T. San-José).

https://doi.org/10.1016/j.cscm.2022.e00906
Received 13 October 2021; Received in revised form 13 January 2022; Accepted 20 January 2022
Available online 22 January 2022

Nomenclature

a	Shear length between load and support points
A	Cross section [mm^2]
A^i_c	"A" of "RC" beam at i-level [mm^2]
A^i_f	"A" of "TRM" element at i-level [mm^2]
A^i_s	"A" of "RB" element at i-level [mm^2]
α_e	E_f / E_m ratio
b	Width of RC beam cross section [mm]
$C1$	"r" strengthened with "$TC1''$
$CB2$	"r" strengthened with "$TCB2''$
$DB2$	"r" strengthened with "$TDB2''$
$DB2U$	"$DB2''$ and U-Shaped
δ_r	Mid-span deflection at "F_r" stage [mm]
δ_{sy}	Mid-span deflection at "F_{sy}" stage [mm]
Δ_r	"M_r" variation compared to "r" [%]
Δ_{sy}	"M_{sy}" variation compared to "r" [%]
E	Young's modulus under pure tensile [GPa]
E_c	Young's modulus of concrete
E_{c1}	"E" in "TRM" (phase I) [GPa]
E_{c2}	"E" in "TRM" (phase II) [GPa]
E_{c3}	"E" in "TRM" (phase III) [GPa]
E_{cm}	Young's Modulus in concrete [GPa]
E_f	"E" of textile [GPa]
F_{sy}	Load when "RB" are yielding [kN]
GDP	Gross Domestic Product [%]
h	Height of RC beam cross section [mm]
H	Measuring distance in TRM tensile test
I_e	Effective section inertia moment
k_t	Factor dependent on load duration
L	Bending test span in "RC" beams
$LVDT$	Linear Variable Differential Transformer
M_a	Bending moment force at mid-span [kN•m]
M_r	Bending moment at "F_r" stage [kN•m]
M_{sy}	Bending moment at "F_{sy}" stage [kN•m]
n	Raised power of Richard and Abbot
n_c	Number of concrete elements
n_f	Number of concrete elements
n_s	Number of "RB"
r	Reference "RC" beams
RB	Reinforcement bars of "RC" beams
RC	Low-grade reinforced concrete
$S1$	"r" strengthened with "$TS1''$
$S1U$	"$S1''$ and U-Shaped
S2	"S1″ plus "TS1″
S3	"S2″ plus "TS1″
SRG	Steel Reinforced Grout
E_m	"E" of mortar [GPa]
E_s	"E" in "RB" [GPa]
ε	Tensile strain
ε^i	Unitary deflection of the i section-level
ε_0	"ε^i" in the highest level of the section
ε_{mc}	"ε" ultimate in "TRM" (phase II)
ε_{mu}	"ε" ultimate in matrix mortar [%]
ε_{su}	"ε" ultimate in "RB" [%]
ε_{sy}	Yield strain of reinforcement bars [%]
$\varepsilon_{t,III}$	"ε" ultimate in "TRM" (phase III)
φ	Curvature of the section
$Ø$	Diameter [mm]
f_0	Stress of Richard and Abbot [MPa]

2019 [1]. This scenario motivated the search for new business niches or to promote existing ones in order to relaunch the construction activity, one of them being Rehabilitation. This subsector has grown in relevance within Spain, but still falls short of European averages. Likewise, the slow, yet progressive ageing of Spanish housing stock brings with it the challenge of rehabilitating several Reinforced-Concrete (RC) structures. The combination of both factors is added stimulus for the investigation of innovative, friendly and cost-effective technologies for the structural retrofitting of these old structures.

This necessity for rehabilitation is recognizable in structures and buildings from the first decades of the 1900 s, years when reinforced concrete started to acquire importance [2]. However, inexperience with the material and the absence of regulations that might otherwise regulate both its design and mix as well as its durability, gave rise to a generation of structures, some of historic value [3], constructed with what is known as lean or low-grade concrete.

The search for an innovative, effective and cost-effective strengthening solution has motivated unstinting investigative efforts among numerous research groups. Organic-matrix composite materials such as Fibre Reinforced Polymer (FRP) emerged at the end of the last century and have within little time opened a breach into a sector firmly committed to traditional solutions. The resistance, lightness, durability and ease of application of these cost-effective materials are their main features [4–8].

The need of this study is based on partially mitigate some of the FRP inconveniences, we may mention: 1) the high cost of the organic matrix if compared with inorganic mortars; 2) its reduced toughness if compared with the TRM ductility (well distributed cracking patterns); 3) low mechanical performance under humid conditions and very hot atmospheres (on the contrary with cement matrixes); and, by extension, 4) its vulnerability to fire [9]. In addition, its application is not recommended for ancient RC structures (i.e. more than 60 aged decayed RC), due to the high rigidity of these composites and high ductility of this type of concrete [10], [11]. As already stated by authors [12], a low-grade RC could be defined as a low-quality material with a compression strength below 17 MPa and, in general, poor mechanical properties because belongs to aged and decayed RC structures.

In consequence, the substitution of the organic matrix for inorganic mortars is presented as a partial improvement in response to the aforementioned problems [13]. With a view to favouring the reinforcing core-matrix interaction, the use of textiles instead of unidirectional fibre sheeting was settled, so mortar can therefore flow through its rovings and cells to consolidate the desired monolithic behaviour. This composite material is called Textile Reinforced Mortar (TRM), and it may be considered as a natural evolution of FRP. Even though it shares the same basic concept of fibres embedded in a matrix, there are many differences between both composite materials.

Since the start of the century, the scientific community has considered the use of textiles to serve as core reinforcement of inorganic matrix composite materials, both in new construction and in rehabilitation. On the one hand, this technology has been used in various studies for the manufacture of prefabricated self-supporting elements [14] or stay-in-space formwork [15], [16]. On the other side, in the field of rehabilitation, TRM was initially introduced for the strengthening of industrial structures such as stone walls and arches [17–20], where promising results were gathered, in view of the difficulty of employing FRP on masonry features. Besides, various research groups are currently studying its use as a structural reinforcement for concrete, although its application in the construction sector is still limited. The investigation of the use of TRM in concrete has been focused on the confinement of columns [21], [22], and

$f_c^{\,i}$	Stress of concrete element at i-level [MPa]
f_{cm}	Compressive strength in concrete [MPa]
f_{ctm}	Indirect tensile strength in concrete [MPa]
$f_f^{\,i}$	Stress of *"TRM"* element at i-level [MPa]
$f_s^{\,i}$	Stress of "RB" element at i-level [MPa]
f_{sy}	Yield stress of *"RB"* [MPa]
f_t	Maximum stress of *"RB"* [MPa]
F_r	Maximum load-bearing capacity [kN]
FRP	Fibre Reinforced Polymer
SRP	Steel Reinforced Polymer
σ	Tensile stress
σ_{mc}	*"σ"* in TRM (phase II)
σ_{mu}	*"σ"* ultimate in matrix mortar [MPa]
$\sigma_{t,III}$	*"σ"* ultimate in TRM (phase III)
TC1	"TRM" with carbon, 1 layer
TCB2	"TRM" with coated basalt, 2 layers
TDB2	"TRM" with denser basalt, 2 layers
TRM	Textile Reinforced Mortar
TS1	"TRM" with steel cords, 1 layer
VBA	Visual Basic Application
V_f	Volumetric fraction of textile
V_m	Volumetric fraction of mortar
y^i	Height of the level under study
y^i_c	"y^i" of concrete material
y^i_f	"y^i" of TRM solution
y^i_s	"y^i" of "RB"

both shear [23], [24] and flexural strengthening [25–27], though few of them involved the strengthening of low-grade concrete [12].

Despite these advances, the implementation of these organic based composites and the use of textiles as inner reinforcements is still far from becoming standard practice in the Construction and/or Rehabilitation sector. A necessary measure to reach this milestone is to characterize the mechanical behaviour of the TRM in order to complete reliable structural calculations [28]. The development of models that can perform satisfactory simulations of RC strengthened components is very important for the development and verification of new strengthening techniques [29]. Several works have proposed numerical models, running on software programs that satisfactorily simulate the behaviour of TRM under tensile. However, their computing time can sometimes be excessive and they often require software programs that are quite expensive.

Easily operated mathematical models are therefore ideal and currently constitute a line of research within the scientific community. In fact, the authors of this work have developed a non-linear model known as the "Cracking Model" [30], which consists of mathematical formulas that are easily replicated. This model is an approach that simulates the TRM stress-strain relationship in pure tensile that was prepared using the results of an experimental campaign. The model was satisfactorily checked with different materials - basalt, carbon and steel cords - acting as TRM core reinforcement, three materials with different stiffness, ultimate strength and strain.

In this study, an easy-to-conduct calculation method was developed to facilitate the design and dimensioning of strengthening interventions with TRM in RC components in flexure. This method, elaborated using Visual Basic Application (VBA) Excel, is based on section-level discretization and the use of the constitutive equation of each material present in the strengthened cross-section. As TRM constitutive equation, the referred "Cracking Model" is used. The idea is to elaborate a final model that can be used with any material as TRM reinforcing core.

This calculation model is checked with the results of a complete experimental campaign centred on the use of TRM as retrofitting material for low-grade concrete beams under flexure. To do so, the present work covers all necessary aspects, theoretical and experimental to achieve a proper modelling. In the first place, the mechanical behaviour of TRM in pure tensile is thoroughly studied. The constituent materials, mortar and used textiles (basalt, carbon and steel cords) are fully characterized, as well as TRM samples tested under unidirectional tensile loads. These last results are contrasted with those provided by the "Cracking Model" to check its suitability. In second place, the results of the direct application of TRM in flexure strengthening to 16 low-grade concrete scaled beams are presented and analysed. Finally, these experimental results are contrasted with those obtained by the calculation method presented within this work.

2. Materials and methods

With a view to subsequent analytical and numerical studies, a proper characterization of the studied composite material (TRM) is important. Not only will the mechanical properties of its constituent materials be tested, but so too will the behaviour of TRM under pure tensile and its strengthening effect on low-grade concrete beams withstanding positive bending moments.

2.1. TRM characteristics

2.1.1. Mortar matrices

The cement-based mortar employed as a matrix of TRM/SRG (sometimes called Steel Reinforced Grout – SRG – when the fabric consists of steel strands) was designed as part of this study, seeking good mechanical performance within acceptable economic manufacturing criteria. Its main characteristics were its maximum aggregate size of 0.6 mm and its content of polymer resins, lower than 4% of volume by weight with the purpose of withstanding fire. The mechanical properties of the mortar were determined through testing, following the curing of 40 × 40 × 160 mm prisms over 28 days, as per UNE-EN 1015–11:2000 [31]. Their average compressive and flexural strength were 20 MPa and 7.2 MPa, respectively.

2.1.2. Reinforcement textiles

As commented upon in the introduction, three materials were employed as internal core reinforcement of the composite material: basalt and carbon fibres as well as steel strands; which are presented in the following four configurations (see Fig. 1). Basalt textiles were supplied by Fife Europe company, while the rest of the materials were purchased to Fidia S.R.L.

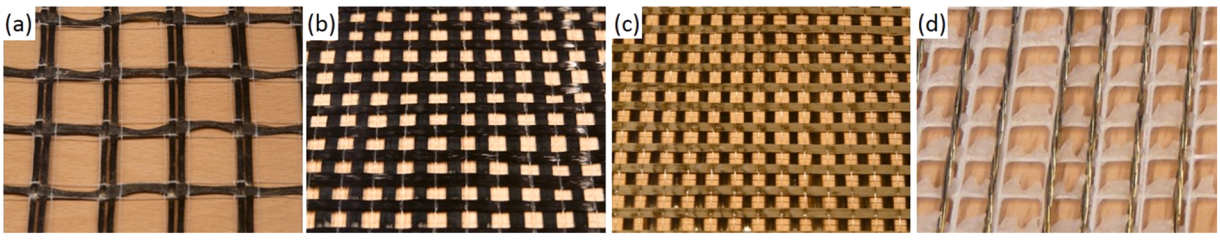

Fig. 1. Textiles: Coated Basalt (a), Denser Basalt (b), Carbon (c) and Steel (d).
Source: Authors.

- Low-density (coated) basalt. The basalt filaments are covered by a bituminous material that generates monolithic rovings which are orthogonally distributed. The surface weight of the textile is 233 g/m^2 and it presents cell sizes of 25 × 25 mm. In this paper, this material will be referred to as "Coated Basalt" (CB).
- Denser basalt. In this case, the basalt filaments are not covered by any material. The distribution of the rovings is also orthogonal and the resulting weight of the textile is 300 g/m^2 with a cell size of 8 × 8 mm. This material is referred to as "Denser Basalt" (DB), to distinguish it from the aforementioned "Coated Basalt".
- Carbon. The bidirectional textile is formed of fibres with an orthogonal distribution. The weight of the textile is 200 g/m^2 uniformly distributed in both directions. The cell dimensions are 8 × 8 mm.
- Steel. Unidirectional textile of drawn steel fibre. Each cord was formed of 5 interwoven strands. An auxiliary polypropylene mesh was used to set the filaments in position with a distribution of 1.57 cords per centimetre. The use of steel fibre is reflected in the name of this composite material: Steel Reinforced Grout (SRG) when the matrix is a mortar and Steel Reinforced Polymer (SRP) when epoxy resins are employed for that purpose. However, the term TRM will generally be employed in this work to avoid confusion.

In Table 1, the mechanical and geometric properties of the above materials are described. These specifications, available from the supplier of the textiles, refer to the individual basalt and carbon fibres and to the steel strands. Clearly, their properties can be notably altered when the textile per se is considered.

Each roving is a yarn of simple fibres known as filaments. A roving is formed of hundreds and even thousands of filaments. The stress-deformation ratio is directly influenced by the position of the filaments and their interaction. Ideally, all the filaments should be positioned in parallel and fully stretched, however the expected performance of both fibres and rovings may differ, depending on the manufacturing method [32]. If we add that numerous rovings act in parallel in a textile, the need may be understood for a mechanical characterization of the textiles employed in this study.

Seven samples of each textile type measuring 600 × 100 mm were tested under uniaxial tensile stress. The specimens were placed in a universal testing machine, with a maximum force of 100 kN and displacement control, which was set at 0.5 mm/min in this test. The elongation of the textile materials was measured by two Linear Variable Differential Transformer (LVDT) sensors that monitored displacement of the clamps that secured the samples. The test data were fed into an MGC-Plus data logger, from the company HBM, at a speed of 50 Hz. The results are summarized in Table 2.

As may be observed in Table 2, the results differed notably from the supplier specifications. Especially surprising was the low performance of both the basalt and the carbon in terms of ultimate tensile strength and strain. This circumstance was attributed to the impossibility of applying the same initial deformation to all of the textile rovings. The distribution of applied force was therefore not constant and premature fracture occurred in the rovings under the heaviest loading [33]. In the case of the steel textile, the ultimate tensile strength was maintained, due to the stiffness of the cords, while greater elongation occurred. The Young's Moduli of the four experimental textiles were considered valid for subsequent analytical calculations.

2.1.3. Tensile test setup

There is no test specified in current standards for the characterization of TRM under pure tensile, thus, authors have chosen a setup similar to those designed by other researchers [34]. The bearing capacity of this composite material under uniaxial tensile loading was investigated using specimens measuring 600 × 100 × 10 mm (see Fig. 2) in a similar way to earlier studies conducted by the same authors [30], [35] or by other research groups [36–39]. Seven samples were manufactured for each of the four materials with two layers of composite's reinforcement for both the basalt textiles due to their low Young's moduli, and one layer of reinforcement for the carbon and steel textiles.

The layout of the fibre rovings and the steel cords was carefully lined up with the longitudinal axis of the specimens. Likewise, two extra textile reinforcements measuring 200 × 100 mm were added at both ends of the samples, in order to facilitate the formation of cracks in the central third of the sample and, in that way, focus the measurement of TRM deformation in that zone, as may be seen in the sketch included in Fig. 3. Thus, a distance (H) of 210 mm was left to measure the actual elongation of the composite material. In the case of the samples with two layers of internal reinforcement, the textiles were equally spaced along the thickness of the cross section.

The specimens were manufactured in plywood formworks and the uniaxial tensile test was conducted after 28 days of controlled curing in a climate chamber. The test was carried out on the same machine that was used to characterize the textiles, using the same displacement rate, 0.5 mm/min. The elongation of the central third of the specimens was measured using two LVDT sensors, located on each side of the specimen, as shown in.

Table 1
Mechanical and geometric properties of the fibres/strand employed as TRM reinforcement.

Property	Coated Basalt	Denser Basalt	Carbon Fibre	Steel Strand
Tensile strength[a] *[MPa]*	2100	3080	3500	3200
Young's Modulus *[GPa]*	89	95	240	206
Ultimate tensile strain *[%]*	3.15	3.15	1.45	1.60
Effectiveness thickness *[mm]*	0.035	0.053	0.056	0.075

[a] Textile effective thickness supplied with manufacturer's specifications.

Table 2
Experimental mechanical properties of the textiles.

Property	Coated Basalt	Denser Basalt	Carbon Fibre	Steel Fibre
Tensile strength[a] *[MPa]*	1160	505	963	3165
Young's Modulus *[GPa]*	67	77	167	160
Ultimate tensile strain *[%]*	1.90	0.84	0.72	2.21

[a] Textile effective thickness supplied with manufacturer's specifications.

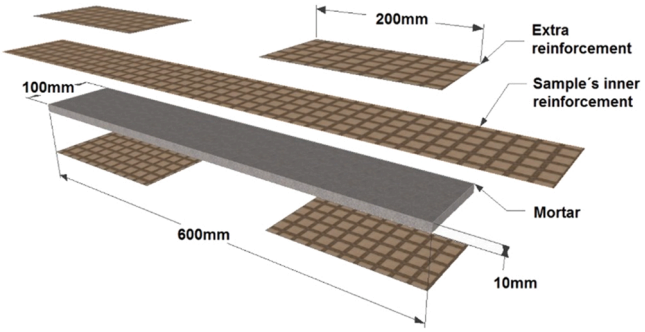

Fig. 2. TRM specimen dimensions for uniaxial tensile test.

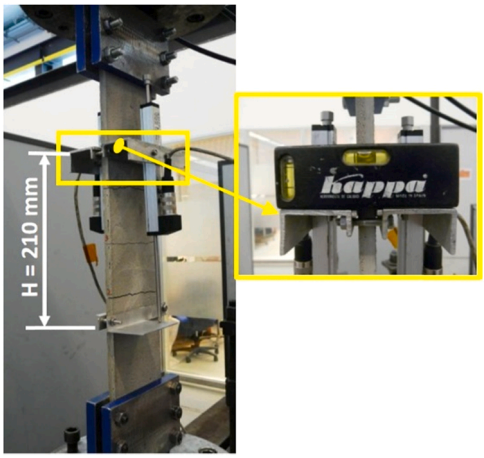

Fig. 3. General view of the TRM uniaxial tensile test.

2.2. Low-grade RC to be strengthened

2.2.1. Low-grade RC beams manufacturing

In this section, several low-grade concrete structural elements are manufactured. A beam structure was chosen for this study the scale of which was reduced to one third of its real dimensions; more specifically, a total of 18 beams (1500 ×150 ×150 mm) were manufactured with a span length of 1.35 m.

With the aim of recreating the mechanical behaviour of the low-grade concrete so often found in older structures, it was decided to use a low-quality concrete with a mean compressive strength ≤ 20 MPa. The cement content of the beams was reduced to 200 kg/cm^3

Table 3
Mean mechanical properties of the used concrete after 28 days curing.

Property	Value
Compressive strength, f_{cm} [MPa]	17.2
Indirect tensile strength, f_{ctm} [MPa]	1.1
Young's Modulus, E_{cm} [GPa]	25.7

using a water/cement ratio of 0.57. The following mechanical characteristics of the concrete were determined after 28 days of curing (see Table 3) using Ø150 × 300 mm cylindrical concrete samples manufactured from the same batch: compressive stress (UNE-EN 12390–2:2009) [40], resistance to indirect tensile (UNE-EN 12390–6:2010) [41] and the Young's modulus (ASTM C 469:2002) [42].

Steel rebars with a diameter of 5 mm class B500T were used for the test samples. The use of this cold-drawn steel as beams longitudinal reinforcement, non-compliant with present standards, had a practical reason. When steel is attacked by chloride ion corrosion (pitting corrosion), the rebars not only sustain an important reduction of their transversal cross sections, their ductility is also adversely affected. Thus, the brittleness of the rebar material increases along with its corrosion and flaking [43]. The authors hence considered it convenient to replicate the behaviour associated with this sort of corrosion that may be appreciated in reinforced concrete structures erected in the first decades of the past century. Therefore, the used steel was characterised according to standard UNE EN 100002–1 [44], the most important properties of which for the analytical calculation are grouped in Table 4.

2.2.2. TRM application in RC beams

This section presents how TRM is installed on above low-grade RC beams [45]. A preliminary treatment of the surface to be strengthened was performed to increase adherence between the composite's mortar and the concrete substrate. With that end in mind, the lower face of each beam was bush hammered, removing the superficial concrete grout and increasing the surface's roughness. The dust produced in the process was evacuated by blowing compressed air. Before the addition of the reinforcement, the rugged surface was wetted to saturation, thereby preventing any partial absorption of water from the fresh mortar of the TRM that might have otherwise altered its mechanical properties and adherence.

The strengthening process consisted of the next steps. Initially, a first layer of fresh mortar (4–5 mm) was extended over the previously treated surface. Then, the textile was installed on the beam, over the fresh mortar. It is advisable to stretch the reinforcement layer as much as possible when it is laid in place to obtain the best possible textile performance, an effect that can be achieved with a roller. Finally, the textile was completely covered with another mortar layer of similar characteristics to the first one. If further textile layers were required, another textile sheet was installed over the fresh grout and the procedure would had continued until the last reinforcing layer was applied. A final mortar grout covered the last installed textile and received a smooth surface finish (see Fig. 4).

In certain samples, U-shaped TRM anchors made from the same material were installed on both ends of the beams to avoid early detachment of the composite, a very common failure mode in externally bonded strengthening solutions [12], [23], [28] (see Fig. 5).

A total of 18 beams scaled down to one third of their original size were tested in this work, two of which both labelled with an "r", served as reference samples and the others were strengthened with different materials and layouts. Two beams of each configuration were tested. Table 5 sets out information on all the beams listed as part of the study: identification code, strengthening material, number of layers applied and use or otherwise of anchors at the ends.

As may be seen, the codes that identified the beams included all the information referring to the strengthening configuration that had been applied. Each label is initially formed of one or two letters that refer to the material used as the TRM core reinforcement; then, there is a number following the prefix of the material that specifies the number of textile layers in use; finally, there may be a letter "U" that indicates whether the beam has U-shaped anchors at both ends. A cardinal number was added after a hyphen to distinguish between both specimens, as there were two sample specimens for each configuration.

2.2.3. Bending test lay-out

The samples were subjected to four-point flexural tests to stimulate the uniformly distributed load behaviour as closely as possible. The distribution of positive flexural stress assumes a trapezoidal form, with a maximum value between the two points of loading. The test was completed on the same universal testing machine employed for the pure tensile test of the TRM, placing the beams on a rigid steel frame. A piston actuator displacement rate of 0.18 mm/min was selected to control the load application. Beam deformation was monitored with the use of 6 LVDTs positioned at key points along its longitudinal axis. All the information was collected by the same MGC-Plus data logger at a sampling rate of 1 Hz.

The test setup, the beam dimensions, the steel reinforcement details and the LVDT positions can be seen in Fig. 6.

Table 4
Mechanical properties of the steel reinforcement bars for manufacturing the beams.

Property	Value
Diameter, *Ø [mm]*	5
Steel yield stress, f_{sy} [MPa]	672
Steel yield strain, ε_{sy} [%]	0.336
Young's Modulus, E_s [GPa]	200
Steel maximum stress, f_t [MPa]	703
Steel ultimate strain, ε_{su} [%]	5.32

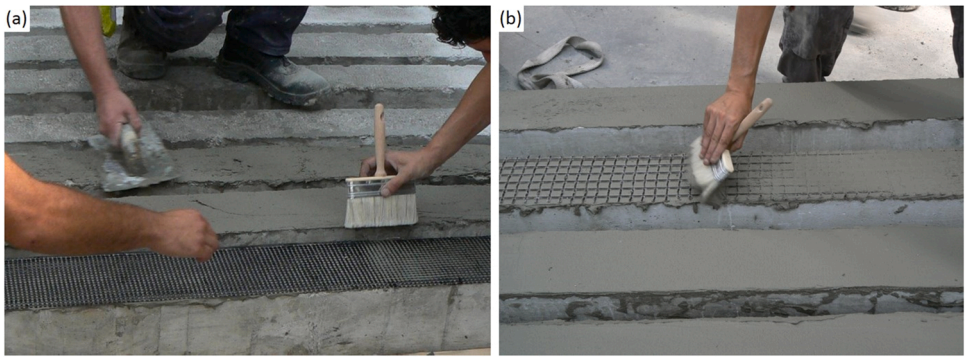

Fig. 4. Application of carbon textile (a) and basalt (b) as internal reinforcement of the TRM.

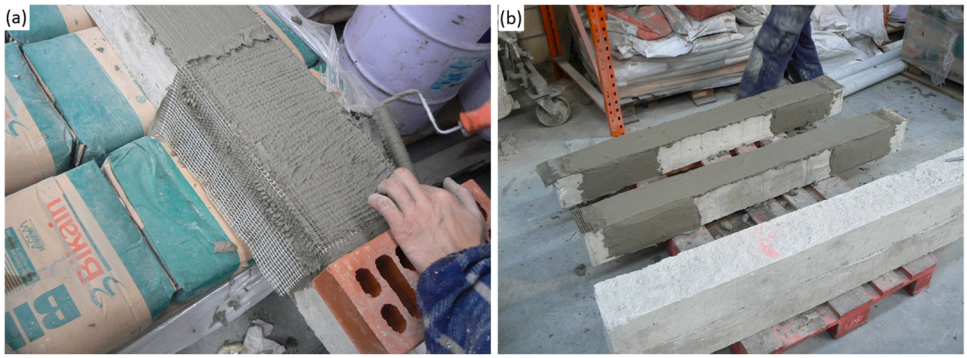

Fig. 5. U-shaped anchors for the beams reinforced with steel fibre (a) and basalt (b) TRM.

Table 5
Descriptive parameters of the beams used in the study.

Strengthening material	Label	num. of layers	Anchors
–	r	–	–
Coated Basalt	CB2	2	–
Denser Basalt	DB2	2	–
	DB2U	2	U-Shaped DB
Carbon	C1	1	–
Steel cords	S1	1	–
	S1U	1	U-Shaped S
	S2	2	–
	S3	3	–

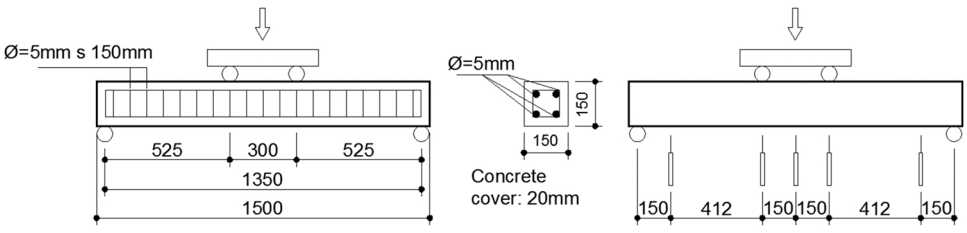

Fig. 6. Test setup, beam geometry, steel reinforcement details (left) and LVDT positions (right).

3. Test results and discussion

3.1. TRM pure tensile test

Adapted from [35], the non-linear tensile behaviour of TRM may be observed in Fig. 7.
Three clearly marked differences can be seen in the graph.

- Phase I: the load is transmitted in a uniform manner across the (mortar and fibre) section. The initial rigidity under tensile stress is basically that of the mortar. This stage ends (σ_{mc}, ε_{mu}) with the appearance of the first crack within the corresponding mortar section.
- Phase II: The load is transmitted through the supporting textile within the cracked sections. In this phase all the cracks are propagated. Their width and separation are directly influenced by the type of internal reinforcement (geometry, section thickness, quantity, content, etc.) and their adherence within the mortar matrix [36]. This phase finishes with the appearance of the final crack in the mortar (σ_{mc}, ε_{mc}).
- Phase III: The last stage is practically linear and the Young's modulus of the composite at this phase is quantified at between 10% and 30% lower than the textile's one [32], [46]. The final failure of the TRM will ($\sigma_{t,III}$, $\varepsilon_{t,III}$) therefore ensue, due to the eventual brittle fracture of the materials employed for internal reinforcement (glass, carbon, aramid, basalt, *etc*.).

The graphs (see Fig. 8) depict similar curves to the one described in Fig. 7. In these graphs, the label designation of each tested sample starts with T from tensile, then describes the type of reinforcing material - CB (coated basalt); DB (basalt denser); C (carbon); and S (steel) -, the number of layers and, finally, the number of the specimen.

The test numerical values are also gathered in Table 6. It again depicts ultimate tensile strength and strain. The value registered for Phase III is included as TRM Young's modulus [36], as that is the phase that will provide the composite's strengthening action in structural applications. This information will be later used for the elaboration of constitutive equations that define the TRM behaviour in pure tensile for subsequent analytical calculations.

As may be observed from the four graphs presented in Fig. 8, the results showed satisfactory repetitiveness, given the type of material that is tested. The development of the curves was similar to the behaviour explained in Fig. 7, distinguishing between the three previously mentioned phases. As the basalt and the carbon textiles were both embedded in the mortar matrix, the ultimate tensile stress and strain values were higher than the figures recorded in the separate textile experimental tests. In this case, the cementitious matrix uniformly distributes the applied load between all the rovings, i.e. all the yarns suffer similar strain [33]. Hence, the drawbacks observed in the textile uniaxial tensile test were avoided and a better effectiveness of the material was achieved.

On the contrary, as expected, the Young's Modulus recorded in phase III of each material was somewhat lower than the experimental modulus of the textile. This reduction ranges from 9% (in the case of denser basalt and steel) to 15% (with carbon fibres) of the experimental values, a fact expected by [32,36,46]. This difference was caused by the presence of the cracks generated in phase II, the width of which increased during phase III, generating stress concentration points and thereby reducing the Young's Modulus of the TRM as a monolithic composite material.

Finally, 7 mortar samples of the same dimensions were prepared without core reinforcement and tested, in order to comprehend the behaviour of the mortar matrix alone under pure tensile load. The following average values were obtained: ultimate tensile strength, $\sigma_{mu} = 2.48$ MPa; ultimate tensile strain, $\varepsilon_{mu} = 0.03\%$; and the Young's modulus, $E_m = 8.25$ GPa.

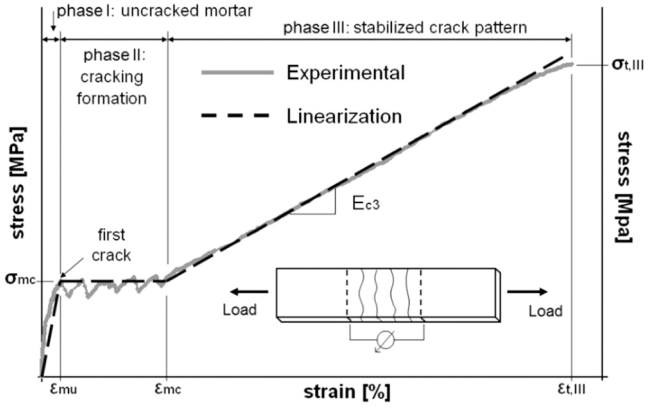

Fig. 7. Stress-strain curve of a TRM specimen under direct tensile-separation.
Adapted from [35].

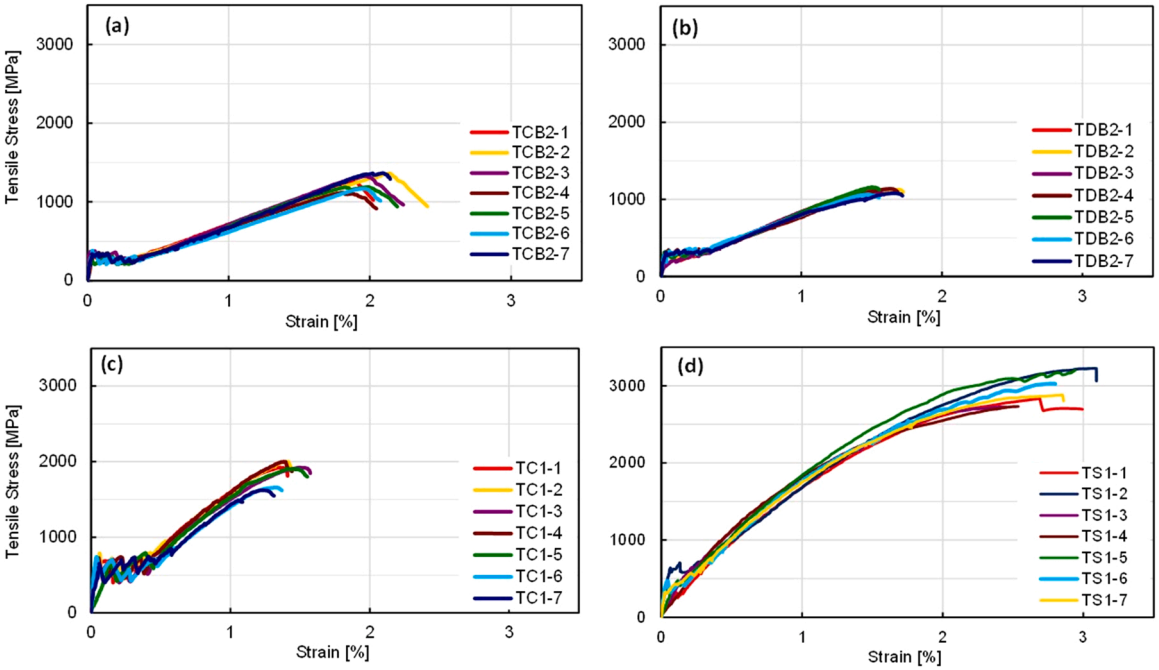

Fig. 8. Stress-strain of TRM with: coated basalt (a), denser basalt (b), carbon (c), and steel fibre (d).

Table 6
Experimental results of TRM specimens under pure tensile.

Property	Coated Basalt	Denser Basalt	Carbon Fibre	Steel Fibre
Tensile strength[a] [MPa]	1256	1111	1865	3165
Young's Modulus [GPa]	59	70	142	144
Ultimate tensile strain [%]	1.97	1.56	1.37	2.76

[a] Textile effective thickness supplied with manufacturer's specifications.

3.2. *Flexural tests of TRM-strengthened RC beams*

The reference beams collapsed following excessive deformation of the rebar framework under tensile load (*Mode 1*), due to the use of the cold-drawn steel. As has been appointed, this failure mode was desired to replicate the brittle failure that may occur in RC beams that suffer from pitting corrosion. On the contrary, in the case of the strengthened beams, three different failure modes were recorded:

- *Mode 2*. Tensile TRM fracture. The TRM core textile reached its maximum elongation and fractured. Breakage of various carbon rovings, following removal of the mortar cover, is shown in Fig. 9a.

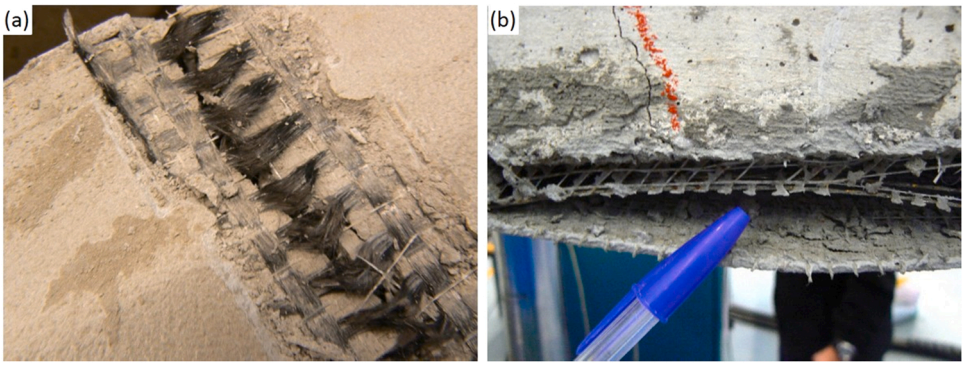

Fig. 9. Fracture of the carbon fibre (a) and premature detachment of the TRM (b), located between two layers of steel reinforcement.

- *Mode 3*. Premature detachment of the TRM. A loss of monolithic behaviour of the composite occurred as the TRM-concrete interface or the inner interfaces between the various layers of core reinforcement material failed, unable to withstand the stress [23]. It is advisable to avoid this failure mode, as it is a type of brittle failure that, in addition, comes with no warning signs. An example of this failure mode is shown in Fig. 9b.
- *Mode 4*. Shear failure at the end of the beam. This catastrophic failure mode occurred unexpectedly in one of the samples, as the beams had been properly designed to withstand these sorts of stresses. The failure was attributed to an unforeseen error in the manufacture of the beam.

As previously described, U-shaped anchors were installed at each end of the beam to mitigate or avoid any loss of the load transfer capacity of the strengthening composite due to premature detachment. Another relevant observation was the variation of the beams' crack pattern. While few and thick cracks appeared in the reference beams, their numbers increased considerably in the reinforced beams and the cracks were finer and more uniformly distributed, all evidence of the better stress distribution due to the TRM [12]. More information related to the deformation of the specimens and the progressive failure process of the retrofitted beams can be found in [12,45,47].

The four possible stages of strengthened RC beams under flexure are shown in Fig. 10. A first stage where the whole section works under flexion until the concrete cracks start to appear. The elastic behaviour of the steel is covered in the second phase. The effect of the externally bonded composite is normally most evident in the third phase (in the graph, a practically horizontal line represents the state of the unreinforced specimens). Finally, the fourth state depicts the behaviour of the element after the failure of the strengthening composite.

In Fig. 11 and Fig. 12 the load-deflection ratios are shown of all the tests on the beams. Given the nature of the materials employed and the type of strengthening technique, of a manual nature, the results presented an acceptable degree of scatter.

In general terms, all the strengthened beams increased their stiffness, load-bearing capacity and ductility with respect to the reference specimens. The stiffness that the TRM contributed was clearly appreciable in the second stage of the curve, i.e. during the elastic phase of the steel rebars, due to the very limited inertia of the transversal section of reinforced concrete (150 ×150 mm). After the steel entered its yield state the general stiffness of the beam decreased, but its load-bearing capacity continued to increase as the deflection increased.

The global results of the experimental campaign are grouped in Table 7. They include the load, the bending moment and the mid-span deflection that were recorded at the instant where the steel reached it elastic limit (F_{sy}, M_{sy} and δ_{sy}) and at the point at which each specimen reached its maximum load-bearing capacity (F_r, M_r and δ_r). The strengthening effect was noticeable in all the cases under study.

The failure mode of the beams strengthened with two layers of coated basalt textile (series CB2) was the fracture of the TRM under tensile (Mode 2), after which the steel rebars of the beam collapsed. In terms of any relative improvement, the load-bearing capacity of the beams in this series increased 33% and 50% with regard to the reference samples.

In contrast, premature detachment (Mode 3) of the TRM occurred on the two beams of the DB2 series, strengthened with two layers of denser basalt. This failure mode was successfully counteracted through the installation of U-shaped anchors at both ends of the beam, achieving the tensile fracture of the TRM (Mode 2) in both beams of the DB2U series. Increased maximum bending moments were recorded for both series that fluctuated between 55% and 75% with regard to the beams used as references.

Likewise, TRM tensile fracture was also identified as the failure mode in the two specimens strengthened with a layer of carbon textile (C1). With this configuration, the increase in the maximum value of the bending moment was quantified at 40% and at 61%.

As shown in Table 7 and Fig. 12, the use of steel fibres showed promising results with regard to an increased load-bearing capacity, stiffness and deformation due to deflection. It is advisable to point out that the data values recorded at mid-span managed to reach 24 mm of deformation as against the 9 mm recorded for the reference samples.

The fragility of premature debonding may be clearly appreciated in Fig. 12a. The S1 series underwent a sudden loss of load-bearing capacity and the consequent failure of their rebar frameworks. However, the application of U-shaped anchors at both ends (S1U series) not only prevented the aforementioned failure but allowed the TRM composite to continue working until tensile failure (Mode 2). In this way, the maximum bending moment and ductility values increased with respect to the series with no anchors. In between both series, reinforced with a single layer of steel textile, increases were recorded for the maximum bending moment that oscillated between

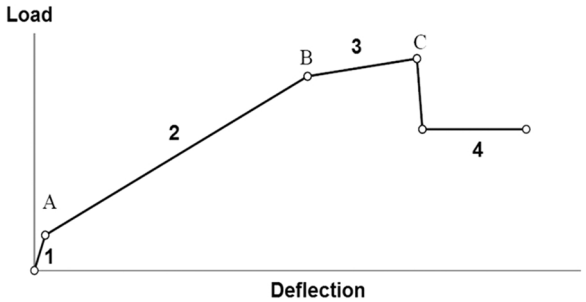

Fig. 10. Behaviour of strengthened RC beams under flexure [48].

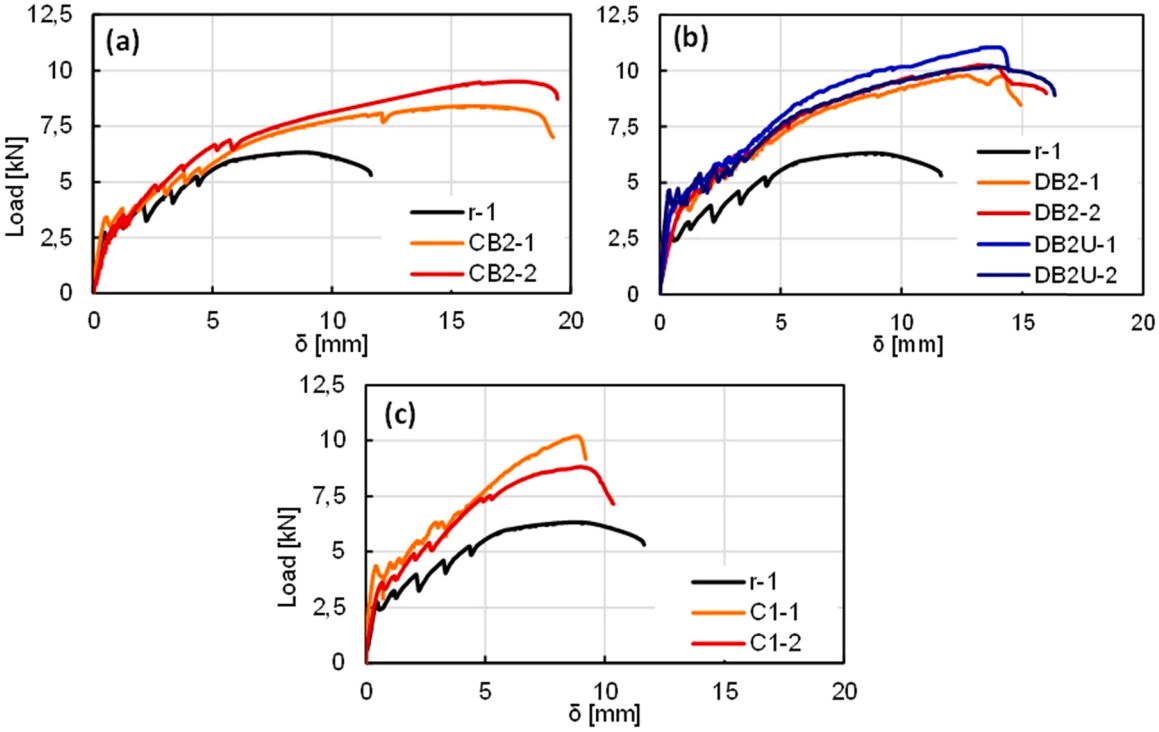

Fig. 11. Load-deflection ratio for coated basalt (a), denser basalt (b) and carbon (c) TRM strengthened beams.

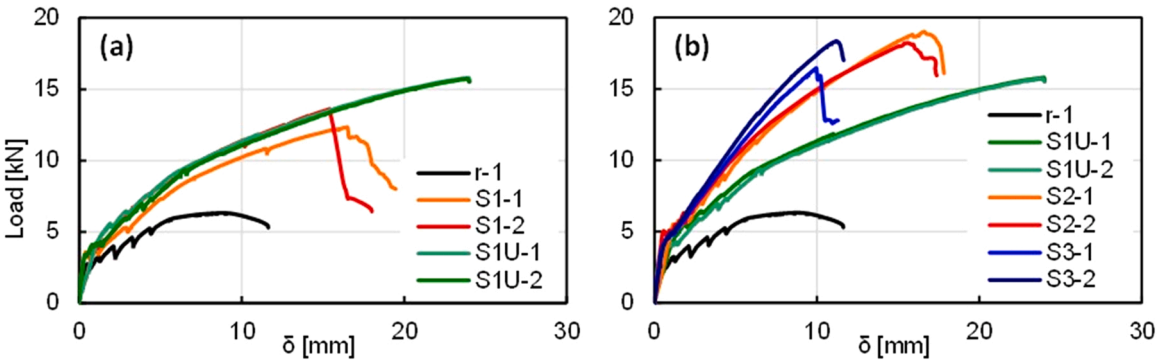

Fig. 12. Load-deflection ratio for steel fibre one layer (a) and various layers (b) TRM strengthened beams.

96% and 150% with regard to the beams with no strengthening.

Finally, Fig. 12b shows the influence of the number of textile layers as TRM inner reinforcement on beam stiffness. However, premature detachment of the strengthening material was observed for both the S2 and the S3 series. Despite this, the effect of the adopted solution on these series strengthened with no U-shaped anchors was satisfactory, as a relevant increase of the maximum bending moment was registered just before the composite detached. This enhancement ranged from 188% to 201% in S2, and from 160% to 190% in S3 series.

4. Analytical modelling

4.1. Introduction

The aim of this section is to develop an easy-to-apply approach to calculate the effect of the TRM as strengthening solution in low-grade RC beams under flexure in a simple, fast and precise way. Therefore, the behaviour of the TRM must be modelled, in order to simulate the composite material in analytical-numerical applications. Thanks to the data that were experimentally obtained, simple mathematical models could accurately reproduce the behaviour that was observed. These models are known as constitutive equations.

Table 7
Summary of the experimental results of the test beams.

Code	F_{sy} [kN]	M_{sy} [kN·m]	Δ_{sy}[a] [%]	δ_{sy} [mm]	F_r [kN]	M_r [kN·m]	Δ_r[a] [%]	δ_r [mm]	Failure mode
r-1	5.84	3.06	–	5.51	6.32	3.32	–	9.16	1
r-2	5.81	3.05	–	5.00	6.48	3.40	–	8.84	1
CB2–1	6.45	3.39	+ 10.7	5.96	8.39	4.41	+ 32.8	15.81	2
CB2–2	6.62	3.48	+ 13.7	5.13	9.51	4.99	+ 50.3	17.88	2
DB2–1	7.98	4.19	+ 36.9	6.26	9.93	5.15	+ 55.1	12.65	3
DB2–2	8.06	4.23	+ 38.2	5.94	10.26	5.39	+ 62.3	13.18	3
DB2U-1	8.54	4.49	+ 46.7	5.76	11.05	5.80	+ 74.6	13.69	2
DB2U-2	8.17	4.29	+ 40.2	5.85	10.20	5.35	+ 61.1	13.65	2
C1–1	8.59	4.51	+ 47.4	5.87	10.20	5.35	+ 61.1	8.31	2
C1–2	7.32	3.84	+ 25.5	4.88	8.83	4.63	+ 39.5	8.99	2
S1–1	8.31	4.36	+ 42.3	6.31	12.36	6.49	+ 95.6	16.49	4
S1–2	8.36	4.39	+ 43.1	5.29	13.26	7.15	+ 115.5	15.41	3
S1U-1	8.86	4.54	+ 51.7	5.75	15.80	8.29	+ 150.0	23.97	2
S1U-2	8.91	4.68	+ 52.6	6.17	15.72	8.25	+ 148.7	23.85	2
S2–1	12.24	6.43	+ 109.5	7.12	19.00	9.97	+ 200.6	16.59	3
S2–2	12.45	6.53	+ 113.2	6.93	18.21	9.56	+ 188.1	15.57	3
S3–1	12.78	6.71	+ 118.8	6.56	16.46	8.64	+ 160.4	9.95	3
S3–2	13.32	6.99	+ 128.1	6.45	18.35	9.63	+ 190.3	11.19	3

[a] Increase of the M_{sy} or M_r compared to the reference beams.

On the other side, the modelling for simulate of beams strengthened with TRM was implemented using VBA Excel, and is based on section-level discretization, according to planes parallel to each other and perpendicular to the flexure plane of the beam under study.

4.2. Constitutive equations of the TRM

The analytical model previously developed by the authors in [30], and known as "Cracking Model", is next applied to the present experimental development. The proposed model is based on the crack control expression from Eurocode 2 [49] and the Aveston–Cooper–Kelly theory (named ACK) [f]; a theory that establishes tri-linear stress–strain curves for reproducing a composite under pure tension (based on a brittle matrix). The former is a non-linear approach developed from a model included in *Eurocode 2 - Part 1* for the calculation of crack thicknesses within reinforced concrete elements under tensile loads. The ACK theory assumes that the fibres are held in the matrix by the only friction forces so that the axial sliding along the interface (fibre–matrix) be possible under a critical, limiting value. Therefore "Cracking Model", is composed on three phases, initially linear, very similar to the stress-strain behaviour explained in the Introduction and detailed in Fig. 7.

The first phase (Phase I) is defined through the law of mixtures, Eq. 1. The Young's modulus of the composite material in this phase, E_{c1}, is a function of the volumetric fraction of the textile, V_f, the volumetric fraction of the mortar, V_m, and of the modules of both components, fibres and mortar, E_f and E_m, respectively. The two last values were experimentally calculated as part of the study here presented.

$$E_{c1} = E_f V_f + E_m V_m \tag{1}$$

Phase II, known as crack formation phase, was simplified through a horizontal line, in other words $E_{c2} = 0$. Knowing that this phase starts when the first crack appears, it is easy to define this point in accordance, once again, with the law of mixtures. Average tensile cracking load of the TRM, σ_{mc}, was obtained with Eq. 2, where the value of mortar resistance to tensile, σ_{mu}, was experimentally calculated, as described in Section 3.1.

$$\sigma_{mc} = (E_{c1} \cdot \sigma_{mu})/E_m \tag{2}$$

To define Phase III constitutive equation it is necessary to use the approach to calculate crack thicknesses in RC components subjected to tensile load included in *Eurocode 2 - Part 1*. If tensile load is applied to a reinforced concrete block, a similar behaviour to the TRM is obtained under the same conditions. The above-mentioned model may therefore be adapted for crack-width calculations, as explained in [30]. Hence, the stress-strain relationship for Phase III is given by Eq. 3:

$$\sigma = (\varepsilon - \varepsilon_{mu}) \cdot E_f + \left(1 + \alpha_e \cdot V_f\right) \cdot k_t \cdot \sigma_{mu}/V_f \tag{3}$$

Where k_t = factor dependent on the load duration, empirically adjusted to 0.2 [30].

$\alpha_e = E_f / E_m$ ratio

This way, knowing the value of σ_{mu} and ε_{mu} obtained experimentally in Section 3.1, the elongation of the composite material at the end of the second phase, ε_{mc}, can be obtained by means of Eq. 4.

$$\varepsilon_{mc} = \left(\sigma_{mc} - \left(1 + \alpha_e \cdot V_f\right) \cdot k_t \cdot \sigma_{mu}/V_f\right)/E_f + \varepsilon_{mu} \tag{4}$$

The model's failure criteria, i.e. TRM ultimate tensile stress ($\sigma_{t,III}$) and its correspondent ultimate strain ($\varepsilon_{t,III}$), is set by the

experimental average ultimate tensile stress recorded in Table 6. The simulations shown in Fig. 13 were obtained from the described equations. Each graphic simulation is superimposed over the experimental results, in grey, for easy comprehension.

In Fig. 13, small differences observable at low strain levels may be overlooked. However, it is very important to control the failure mode in this type of strengthening solutions, as is highlighted by other authors [39], [50], who points out the importance of preventing large discrepancies throughout the rest of the simulation, especially at the failure stage. It can likewise be seen that the straight line in representation of Phase III in the model is progressively divergent from the grey area that covers the experimental results. This difference is especially obvious in the results of the composite material reinforced with steel textile.

With a view to improving the results of the proposed model, a correction was introduced based on Richard and Abbot [51] expression, as presented in Eq. 5. With this correction, widely employed in the simulation of reinforced concrete [52], the aim is to fine-tune the model in the failure zone, considering that the phase close to failure of the composite material will tend not to be sloped on the graph.

$$f_c = \frac{((E_1 - E_2)\cdot \varepsilon_c)}{\left(1 + \left((E_1 - E_2)\cdot \frac{\varepsilon_c}{f_0}\right)^n\right)^{1/n}} + E_2 \cdot E\varepsilon_2 \tag{5}$$

Eqs. 3 and 5 were combined to form Eq. 6. For E_1, the Young's modulus of the textile, E_f, was chosen. It was likewise considered that the final phase of the experimental curves is asymptotic with an imaginary horizontal line, which explains why E_2 was given a null value. Therefore, f_0 reflects the localization of this line parallel to the x-axis. Its value was set at the ultimate tensile strength that the TRM reached in the experimental test, values that are included in Table 6 ($\sigma_{t,III}$). On the other side, the raised power of n is established empirically [30]. With all, Eq. 6 was formulated as:

$$\sigma = \frac{\left((\varepsilon - \varepsilon_{mu})\cdot E_f\right)}{\left(1 + \left((\varepsilon - \varepsilon_{mu})\cdot \frac{E_f}{f_0}\right)^n\right)^{1/n}} + \left(1 + \alpha_e \cdot V_f\right)\cdot k_t \cdot \sigma_{mu} \Big/ V_f \tag{6}$$

After applying this correction, a better correlation between the experimental results and the outcomes of the proposed approach may be seen from the graphs included in Fig. 14.

In the following section, this model's efficacy will be tested through a simple numerical application that simulates the behaviour of the beams strengthened and tested in this work.

4.3. 4.3 Simulation of beams strengthened with TRM

The concrete cross section is divided into 52 rectangular elements such as may be seen in Fig. 15.

The steel and the installed TRM are associated with the level at which they are placed. The constitutive equation of the concrete under compressive forces can be found in Eurocode2 - Part 1.1 [49], whereas the Park and Paulay model [53], widely used in this kind of simulation, was used to replicate the steel rebars behaviour because, among others available such as elasto-plastic, bilinear and trilinear models, [54] and [55],authors selected Park-Paulay's model, due to the optimum balance between the complexity of its equations and its satisfactory correlation with experimental results. On the other hand, the "Cracking model" was applied to simulate the TRM. It can be noted, that this model can be used with other composites, such as FRP, as long as its constitutive equation is known.

At a certain level of deformation, the model calculates, through an iterative process, the longitudinal deflection at all the defined levels and, through the use of constitutive equations, the force related with that deflection that guarantees the equilibrium of the section. Through the curvature concept, φ, and starting from the deformation at highest level of the section, ε_o, deformation at all discretized levels can be obtained through Eq. 7 and the Bernoulli Hypothesis. Which establishes that, ongoing pure bending, the plane sections perpendicular to the longitudinal axis of the beam before deflection, continued plain and perpendicular to the beam longitudinal axis following deflection [56].

$$\varepsilon^i = \varepsilon_0 + \varphi \cdot y^i \tag{7}$$

Where:

ε^i = unitary deflection of the level under study.

ε_o = unitary deflection of the highest level of the section.

φ = curvature of the section.

y^i = height of the level under study.

Having defined all the deflections, materials' constitutive equations are used to determine the corresponding stresses (f^i_c - concrete, f^i_f - TRM and f^i_s - Reinforcement bars) applied in respective i-element sections (A^i_c - concrete, A^i_f - TRM and A^i_s - Reinforcement bars), within the elements that ensure equilibrium (Eqs. 8 and 9). Finally, in this way, the resulting bending moment of the cross section can be found.

$$N = \sum_{i=1}^{nc} f_c{}^i A_c{}^i + \sum_{i=1}^{ns} f_s{}^i A_s{}^i + \sum_{i=1}^{nf} f_f{}^i A_f{}^i \tag{8}$$

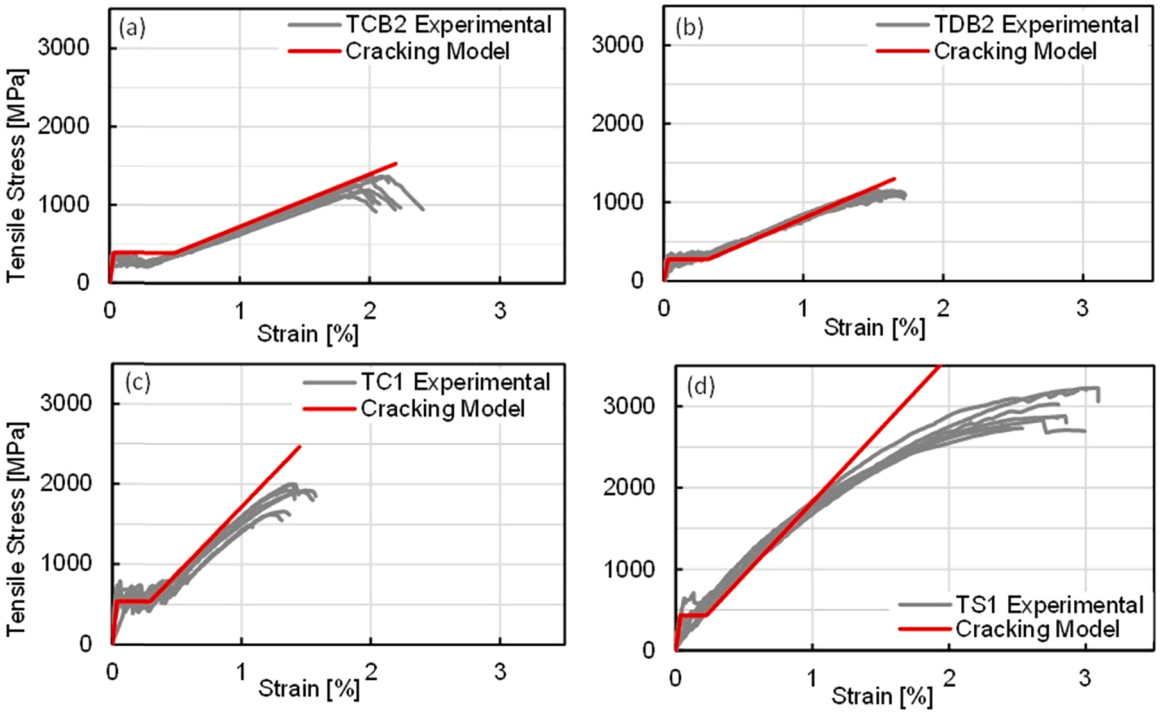

Fig. 13. Initial comparison of "Cracking Model" vs experiments of: coated basalt (a), denser basalt (b), carbon (c) and steel fibres (d).

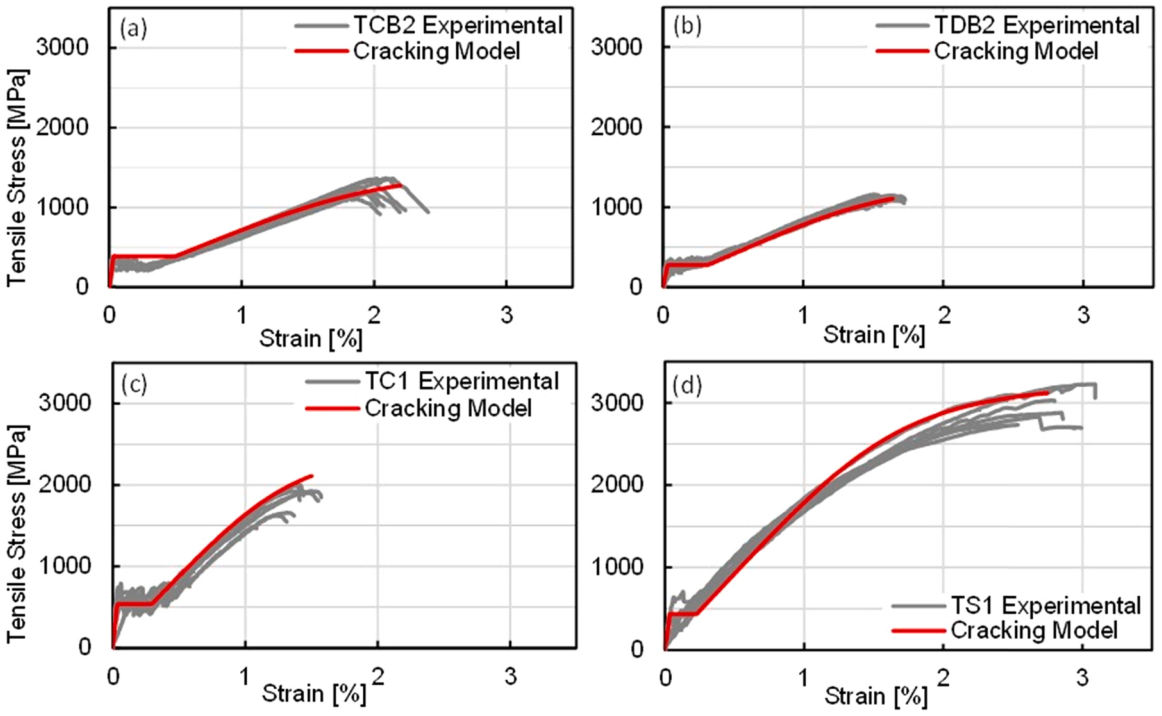

Fig. 14. Final comparison of the "Cracking Model" vs experiments of: coated basalt (a), denser basalt (b), carbon (c) and steel fibres (d).

$$M = \sum_{i=1}^{nc} f_c{}^i A_c{}^i y_c{}^i + \sum_{i=1}^{ns} f_s{}^i A_s{}^i y_s{}^i + \sum_{i=1}^{nf} f_f{}^i A_f{}^i y_f{}^i \tag{9}$$

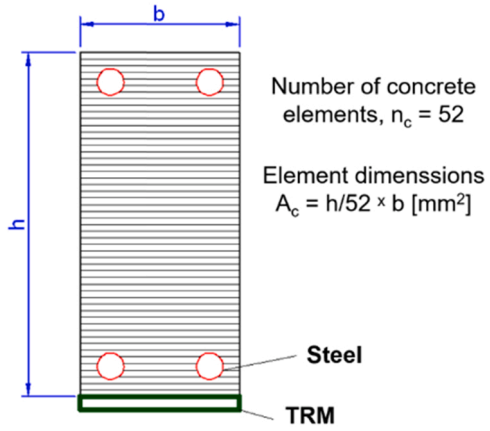

Fig. 15. Section discretization for the numerical simulation.

The deflection at mid-span for bi-supported beams undergoing four-point flexural testing is calculated through Eq. 10 in accordance with the specifications of the Spanish Structural Concrete Code EHE-08 [57].

$$\delta_{flexure} + \delta_{shear} = \frac{(3L^2 - 4a^2)M_a}{24E_c \cdot I_e} + \frac{M_a \cdot h^2}{10G_c \cdot I_e} \tag{10}$$

Due to the low shear stress values observed in the tested geometric configuration, the contribution done by the shear stress to the total deflection is neglected (less than 1% of the final sum). In consequence, only the first addend from Eq. 10 was employed.

Where M_a = bending moment force at mid-span.

L = bending test span.

a = shear length, distance between one point of load application and its closest support point.

E_c = concrete modulus of elasticity.

I_e = effective section inertia moment.

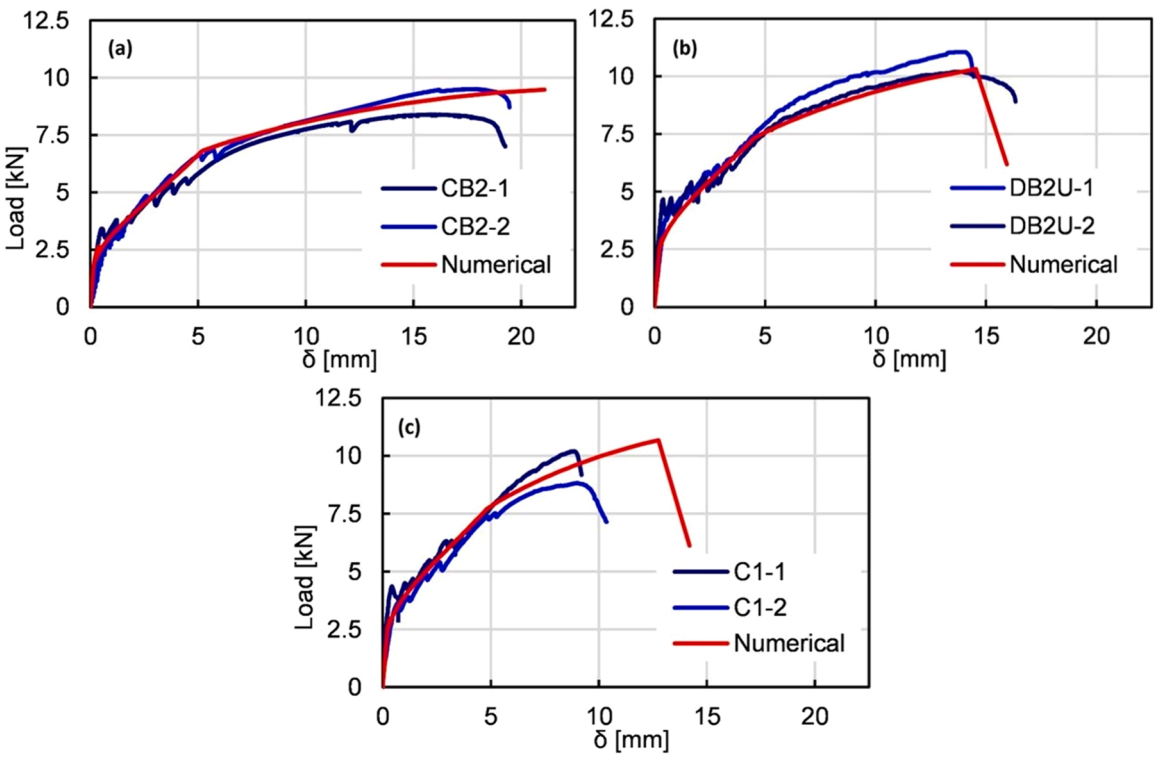

Fig. 16. Numerical simulation of beams strengthened with TRM: coated basalt (a), denser basalt (b) and carbon (c).

The Branson method [58] is recommended in the Spanish Code (EHE-08), among other current approaches, to finding the value of I_e. It is also included in ACI 318 building code. This approximation is valid for deflection calculations within the elastic limits of the steel bars. Following their plastic deformation, in order to simulate the beams deflection, the authors devised an interpretation of the plastic-hinge theory based on the formula proposed by Esmaeily [55], which was adapted ad hoc to the tested beams. The results of the simulation are shown below in Fig. 16 and Fig. 17.

From the results presented in Fig. 16, where the simulations of the series strengthened with basalt and carbon textiles (series CB2, DBU2 and C1) are shown, the way in which the model completed a satisfactory simulation of the experimental results can be seen, especially in terms of stiffness in phases 1, 2 and 3 (see Fig. 10). As TRM premature detachment is not considered as a failure mode in this method, the corresponding numerical results for DB series were compared with the samples strengthened with U-shaped anchors. In this series the tensile fracture of the composite was achieved, a failure mode that the model can prevent.

It may be pointed out that the modelling of the C1 series beams (Fig. 16c) predicted tensile fracture of the TRM textile core reinforcement at a higher deformation rate than the experimental result. This difference might imply that the failure mode of the tested specimens was not only due to the tensile fracture of the TRM, but that it was a combination with another failure mode that, for example, may have produced a loss of monolithic behaviour within the TRM composite material [59]. As it was not a coated textile, the cement matrix only adhered to the external fibres of the roving, so that the transfer of stress to the internal fibres of the very roving was solely due to friction. This fact can provoke the so-called "sleeve effect" [60], in other words, a situation in which the internal fibres of a roving are not deformed to quite the same proportion as the external ones, which undergo the same deformation as TRM and beam. In this way, a homogeneous distribution of the stresses is not produced, so the external fibres may reach the ultimate tensile failure state quicker, thereby resulting in an inferior performance of the textile.

Satisfactory results from the simulation for the beams strengthened with steel fibre were also obtained (Fig. 17). As in the samples strengthened with one layer (series S1) premature detachment of the TRM was registered, the model outcomes were compared with the experimental results of series S1U where the steel fibre TRM did achieve tensile fracture. In Fig. 17a, it may be seen that the model generated satisfactory failure predictions for that series. Likewise, the failure modes of the beams from both the S2 and the S3 series were also due to premature TRM debonding, a circumstance that the proposed model does not yet consider (Fig. 17b and c). Even so, the model satisfactorily simulated the behaviour of the reinforced beams until that undesired detachment took place in the experimental tests.

4.4. *Accuracy of the analytical modelling vs experimental results*

The cracking model from authors [30], based on Eurocode 2 [49] and the ACK theory [61], reproduces quite well the experimental results for the TRM under pure tension loads. However, a correction was introduced [51], as usual for calculating RC structures [52], in

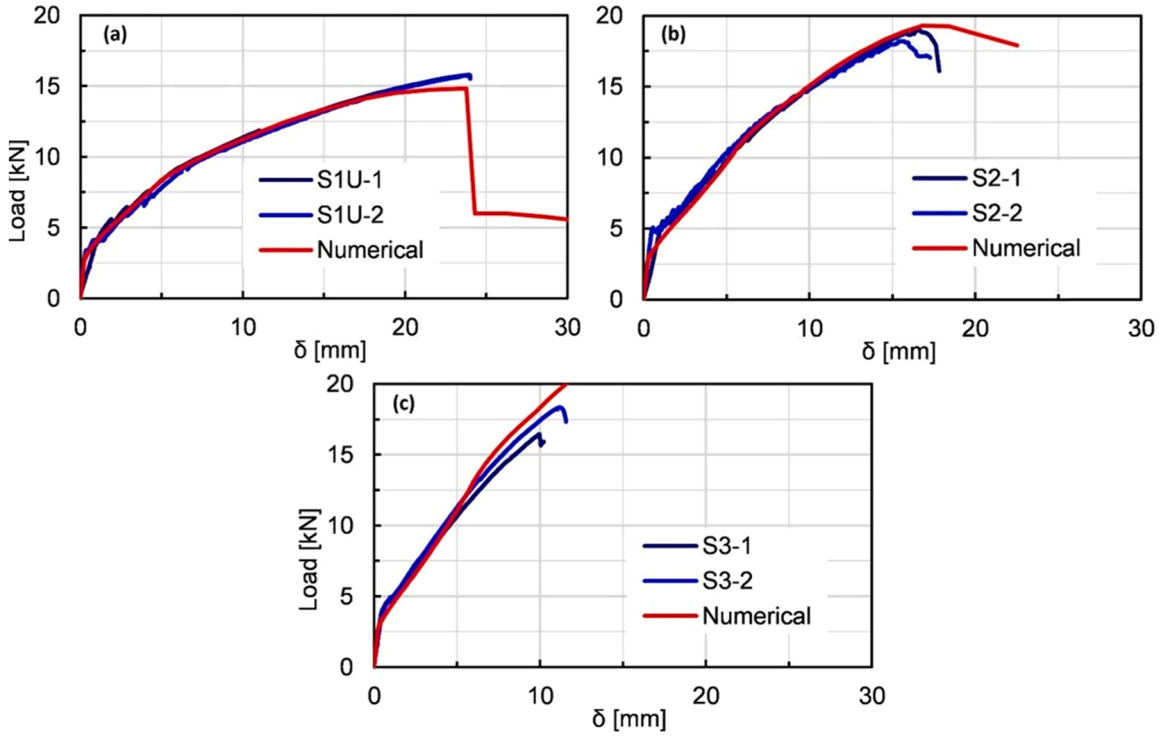

Fig. 17. Numerical simulation of beams strengthened with steel fibre TRM: one reinforcement layer (a), two layers (b) and three layers (c).

order to improve this model in the failure zone (ultimate tension loads) of TRM composite. Therefore, the TRM failure model here verified, according to the present experimental study, can be employed as a constitutive equation of the TRM with regard to analytical-numerical applications, in which the effects of this composite are analysed as a strengthening system for low-grade RC components in flexure.

Additionally, the modelling of TRM strengthened beams for bi-supported elements undergoing four-point flexural testing, based on section-level discretization, reproduces quite well the archived experimental results but bearing in mind the following assumptions: the Branson [58] method approximation, the plastic-hinge theory based on the formula proposed by Esmaeily [55] and, finally, not considering as a failure mode the premature TRM detachments.

As a concluding remark, more exhaustive study of the materials might lead to the elaboration of coefficients for a calculation method mainly based on the properties of the basic materials that make up the composite. Likewise, deeper knowledge must be gained in the future through studies on the TRM-concrete interface and its behaviour, so as to prevent premature detachment of the strengthening material.

5. Conclusions

This work presents an easy-to-conduct numerical approach to assess the behaviour of low-grade reinforced concrete beams (<17 MPa) retrofitted in flexure with Textile Reinforced Mortar (TRM). To support that aim, the produced numerical results are compared to those obtained on the testing of 16 scaled beams strengthened in flexure. In this experimental campaign various types of TRM configurations proved their effectiveness. Depending on the composite material and configuration used, the maximum bending moment has increased between 30% and 200% with respect to the reference beams.

All the strengthened beams with TRM increased their stiffness, load-bearing capacity and ductility with respect to the reference ones. The TRM stiffness contribution was appreciable during the elastic phase of the steel rebars, due to the low inertia of the transversal section of RC beams. Once the steel rebars yielded, the general stiffness of the beam decreased, but its load-bearing capacity continues rising as the deflection increased.

Different failure modes have likewise been observed. The failure mechanism related with the loss of strengthening action, due to undesired premature detachment, was effectively countered using U-shaped anchors. This effect was especially noticeable in the specimens strengthened with a layer of steel fabric. The presence of U-shaped anchors at both ends led to the tensile TRM fracture therefore increasing by 23% the strengthening capacity of the applied solution and by 50% the ductility of the retrofitted beam when compared with specimens with no U-shaped anchors.

The TRM composite has been properly characterized under pure tensile applying a model previously developed by the authors known as “Cracking Model”, whose results have been also contrasted with the experimental ones. The development of the pure tension curves clearly distinguish the three phases: I- based on the rigidity tensile stress of the mortar, II- the load is transmitted through textile core (cracked sections) and, finally, III- linear being the Young’s modulus of TRM between 10% and 30% lower than the textile’s one, an effect caused by the phase II cracking whose widths increased in phase III, generating stress concentration points and thereby reducing the Young’s Modulus of the TRM as a monolithic composite material.

The numerical analysis of the beams strengthened with TRM has shown satisfactory results, according to the present experimental study. The “Cracking Model” here verified is able as a constitutive equation of the TRM with regard to analytical-numerical applications, in which the effects of this composite are analysed as a strengthening system for low-grade RC components in flexure. It may be pointed out that in the coated textiles, as carbon TRM, the cement matrix only adhered to the external fibres of the roving, so that the transfer of stress to the internal fibres of the very roving was solely due to friction, provoking the “sleeve effect”. In this case, a homogeneous distribution of the stresses is not produced, so the external fibres may reach the ultimate tensile failure state quicker, resulting in a lower TRM core (textile) performance. Additionally, the proposed model does not consider premature TRM debonding, even so, this model satisfactorily simulated the behaviour of the reinforced beams until that undesired detachment took place in experiments. Thus, deeper knowledge must be gained in the future through studies on the TRM-concrete interface and its behaviour, so as to prevent premature detachment of the strengthening material.

Declaration of Competing Interest

The authors declare that they have no known competing financial interests or personal relationships that could have appeared to influence the work reported in this paper.

Acknowledgements

The authors wish to express their gratitude to the support received from Morteros y Revocos Bikain, S.A. (IDI-20101594) and Orion Reparación Estructural S.L. (IDI-20101592) within the framework of TERREME project. Our thanks also go to MCIN/AEI/10.13039/501100011033/ FEDER, UE [PID2021–124203OB-I00 and RTI2018–097079-B-C31] and, finally, to SAREN research group (IT1619–22, the Basque Government).

References

[1] Instituto Nacional de Estadística (INE). Statistics National Institute of Spain, 'España en cifras 2020', 2020. http://www.ine.es/prodyser/espa_cifras(ISSN 2255–0410.

[2] I. Marcos, J.-T. San-José, L. Garmendia, A. Santamaría, J.M. Manso, Central lessons from the historical analysis of 24 reinforced-concrete structures in northern Spain, J. Cult. Herit. 20 (2016) 649–659, https://doi.org/10.1016/j.culher.2016.03.003.

[3] I. Marcos, J.-T. San-José, A. Santamaría, L. Garmendia, 'Early concrete structures: patented systems and construction features, Int. J. Archit. Herit. vol. 12 (2018) 310–319.

[4] S.S. Zhang, Y. Ke, S.T. Smith, H.P. Zhu, Z.L. Wang, Effect of FRP U-jackets on the behaviour of RC beams strengthened in flexure with NSM CFRP strips, Compos. Struct. 256 (2021), 113095, https://doi.org/10.1016/j.compstruct.2020.113095.

[5] R. Haghani, M. Al-Emrani, R. Kliger, A new method for strengthen concrete structures using prestressed FRP laminates, Proc. Int. Struct. Eng. Constr. 2 (1) (2015), https://doi.org/10.14455/ISEC.res.2015.211.

[6] K. Chaiyasarn, Q. Hussain, P. Joyklad, K. Rodsin, New hybrid basalt/E-glass FRP jacketing for enhanced confinement of recycled aggregate concrete with clay brick aggregate, Case Stud. Constr. Mater. 14 (2021), e00507, https://doi.org/10.1016/j.cscm.2021.e00507.

[7] A. Mofidi, O. Chaallal, Shear strengthening of RC beams with EB FRP: influencing factors and conceptual debonding model, J. Compos. Constr. 15 (1) (2011) 62–74, https://doi.org/10.1061/(ASCE)CC.1943-5614.0000153.

[8] Q. Hussain, A. Ruangrassamee, S. Tangtermsirikul, P. Joyklad, A. Wijeyewickrema, Low-cost fiber rope reinforced polymer (FRRP) confinement of square columns with different corner radii, Buildings 11 (2021) 355, https://doi.org/10.3390/buildings11080355.

[9] H.M. Elsanadedy, H. Abbas, T.H. Almusallam, Y.A. Al-Salloum, Organic versus inorganic matrix composites for bond-critical strengthening applications of RC structures – State-of-the-art review, Compos. Part B Eng. 174 (2019), 106947, https://doi.org/10.1016/j.compositesb.2019.106947.

[10] T. Triantafillou, Strengthening of existing concrete structures: Concepts and structural behavior, Chapter 13, in: T. Triantafillou (Ed.), Textile Fibre Composites in Civil Engineering, Woodhead Publishing, 2016, pp. 303–322, https://doi.org/10.1016/B978-1-78242-446-8.00014-8. Chapter 13.

[11] L.G. Arrieta, I.M. Rodríguez, N.L. Arlanzón, E.B. Blanco, 'Damage assessment and conservation strategy for the largest covered market in Europe: the Ribera Market (Bilbao, Int. J. Archit. Herit. 12 (6) (2018) 997–1018, https://doi.org/10.1080/15583058.2018.1431728.

[12] P. Larrinaga, L. Garmendia, I. Piñero, J.-T. San-José, Flexural strengthening of low-grade reinforced concrete beams with compatible composite material: Steel Reinforced Grout (SRG), Constr. Build. Mater. 235 (2020), 117790, https://doi.org/10.1016/j.conbuildmat.2019.117790.

[13] T. Triantafillou, Strengthening of existing masonry structures: Concepts and structural behavior, Chapter 15, in: T. Triantafillou (Ed.), Textile Fibre Composites in Civil Engineering, Woodhead Publishing, 2016, pp. 361–374, https://doi.org/10.1016/B978-1-78242-446-8.00016-1. Chapter 15.

[14] E. Tsangouri, A. Van Driessche, G. Livitsanos, D.G. Aggelis, Design, casting and fracture analysis of textile reinforced cementitious shells, Dev. Built Environ. 3 (2020), 100013, https://doi.org/10.1016/j.dibe.2020.100013.

[15] S. Li, S. Yin, The influence of the bonding length on the failure mechanism of the interface between the TRC permanent formwork and cast-in-place concrete, Structures 29 (2021) 1690–1698, https://doi.org/10.1016/j.istruc.2020.11.080.

[16] H.-Y. Kim, et al., Load-deflection behaviour of concrete slab-type elements casted on stay-in-place TRC formwork, Compos. Struct. 244 (2020), 112310, https://doi.org/10.1016/j.compstruct.2020.112310.

[17] L. Garmendia, P. Larrinaga, R. San-Mateos, J.T. San-José, Strengthening masonry vaults with organic and inorganic composites: an experimental approach, Mater. Des. 85 (2015) 102–114, https://doi.org/10.1016/j.matdes.2015.06.150.

[18] D. García, J.T. San-José, L. Garmendia, P. Larrinaga, Comparison between experimental values and standards on natural stone masonry mechanical properties, Constr. Build. Mater. 28 (1) (2012) 444–449, https://doi.org/10.1016/j.conbuildmat.2011.08.012.

[19] P. Meriggi, G. de Felice, S. De Santis, Design of the out-of-plane strengthening of masonry walls with fabric reinforced cementitious matrix composites, Constr. Build. Mater. 240 (2020), 117946, https://doi.org/10.1016/j.conbuildmat.2019.117946.

[20] L. Mercedes, E. Bernat, L. Gil, In-plane cyclic loading of masonry walls strengthened by vegetal-fabric-reinforced cementitious matrix (FRCM) composites, Eng. Struct. 221 (2020), 111097, https://doi.org/10.1016/j.engstruct.2020.111097.

[21] S.-H. Park, N.H. Dinh, J.-W. Um, K.-K. Choi, Experimental study on the seismic performance of RC columns retrofitted by lap-spliced textile-reinforced mortar jackets after high-temperature exposure, Compos. Struct. 256 (2021), 113108, https://doi.org/10.1016/j.compstruct.2020.113108.

[22] A.N. Al-Gemeel, Y. Zhuge, Using textile reinforced engineered cementitious composite for concrete columns confinement, Compos. Struct. 210 (2019) 695–706, https://doi.org/10.1016/j.compstruct.2018.11.093.

[23] S.M. Raoof, D.A. Bournas, TRM versus FRP in flexural strengthening of RC beams: behaviour at high temperatures, Constr. Build. Mater. 154 (2017) 424–437, https://doi.org/10.1016/j.conbuildmat.2017.07.195.

[24] Z.C. Tetta, L.N. Koutas, D.A. Bournas, Shear strengthening of full-scale RC T-beams using textile-reinforced mortar and textile-based anchors, Compos. Part B Eng. 95 (2016) 225–239, https://doi.org/10.1016/j.compositesb.2016.03.076.

[25] H.M. Elsanadedy, T.H. Almusallam, S.H. Alsayed, Y.A. Al-Salloum, Flexural strengthening of RC beams using textile reinforced mortar – Experimental and numerical study, Compos. Struct. 97 (2013) 40–55, https://doi.org/10.1016/j.compstruct.2012.09.053.

[26] A. de, A. Vieira, S.P. Triantafyllou, D.A. Bournas, Strengthening of RC frame subassemblies against progressive collapse using TRM and NSM reinforcement, Eng. Struct. 207 (2020), 110002, https://doi.org/10.1016/j.engstruct.2019.110002.

[27] S.M. Raoof, L.N. Koutas, D.A. Bournas, Textile-reinforced mortar (TRM) versus fibre-reinforced polymers (FRP) in flexural strengthening of RC beams, Constr. Build. Mater. 151 (2017) 279–291, https://doi.org/10.1016/j.conbuildmat.2017.05.023.

[28] G. Cai, K.D. Tsavdaridis, A. Si Larbi, P. Purnell, A simplified design approach for predicting the flexural behavior of TRM-strengthened RC beams under cyclic loads, Constr. Build. Mater. 285 (2021), 122799, https://doi.org/10.1016/j.conbuildmat.2021.122799.

[29] X. Wang, C.C. Lam, V.P. Iu, Bond behaviour of steel-TRM composites for strengthening masonry elements: experimental testing and numerical modelling, Constr. Build. Mater. 253 (2020), 119157, https://doi.org/10.1016/j.conbuildmat.2020.119157.

[30] P. Larrinaga, C. Chastre, J.T. San-José, L. Garmendia, Non-linear analytical model of composites based on basalt textile reinforced mortar under uniaxial tension, Compos. Part B Eng. 55 (2013) 518–527, https://doi.org/10.1016/j.compositesb.2013.06.043.

[31] 'UNE-EN 1015–11:2000/A1:2007, Methods of Test for Mortar for Masonry - Part 11: Determination of Flexural and Compressive Strength of Hardened Mortar'. AENOR.

[32] J. Hegger, et al., Mechanical Behaviour of Textile Reinforced Concrete. in State-of-the-Art report of RILEM Technical Committee TC 201-TRC 'Textile Reinforced Concrete', RILEM Publ, Bagneux, 2006.

[33] G. Ferrara, M. Pepe, E. Martinelli, R.D. Tolêdo Filho, Tensile behavior of flax textile reinforced lime-mortar: Influence of reinforcement amount and textile impregnation, Cem. Concr. Compos. 119 (2021), 103984, https://doi.org/10.1016/j.cemconcomp.2021.103984.

[34] M. Lee, J. Mata-Falcón, W. Kaufmann, Load-deformation behaviour of weft-knitted textile reinforced concrete in uniaxial tension, Mater. Struct. 54 (2021), https://doi.org/10.1617/s11527-021-01797-5.

[35] P. Larrinaga, C. Chastre, H.C. Biscaia, J.T. San-José, Experimental and numerical modeling of basalt textile reinforced mortar behavior under uniaxial tensile stress, Mater. Des. 55 (2014) 66–74, https://doi.org/10.1016/j.matdes.2013.09.050.

[36] C. Caggegi, E. Lanoye, K. Djama, A. Bassil, A. Gabor, Tensile behaviour of a basalt TRM strengthening system: influence of mortar and reinforcing textile ratios, Compos. Part B Eng. 130 (2017) 90–102, https://doi.org/10.1016/j.compositesb.2017.07.027.

[37] S. De Santis, G. de Felice, Tensile behaviour of mortar-based composites for externally bonded reinforcement systems, Compos. Part B Eng. 68 (2015) 401–413, https://doi.org/10.1016/j.compositesb.2014.09.011.

[38] F.G. Carozzi, C. Poggi, Mechanical properties and debonding strength of Fabric Reinforced Cementitious Matrix (FRCM) systems for masonry strengthening, Compos. Part B Eng. 70 (2015) 215–230, https://doi.org/10.1016/j.compositesb.2014.10.056.

[39] Z. Dong, M. Deng, C. Zhang, Y. Zhang, H. Sun, Tensile behavior of glass textile reinforced mortar (TRM) added with short PVA fibers, Constr. Build. Mater. 260 (2020), 119897, https://doi.org/10.1016/j.conbuildmat.2020.119897.
[40] 'UNE-EN 12390–3:2009, Testing Hardened Concrete - Part 3: Compressive Strength of Test Specimens'. AENOR.
[41] 'UNE-EN 12390–6:2010, Testing Hardened Concrete - Part 6: Tensile Splitting Strength of Test Specimens'. AENOR.
[42] 'ASTM C 469:2002, Standard Test Method for Static Modulus of Elasticity and Poisson's Ratio of Concrete in Compression'. American Society for Testing and Materials.
[43] R. Songbo, G. Ying, K. Chao, G. Song, X. Shanhua, Y. Liqiong, Effects of the corrosion pitting parameters on the mechanical properties of corroded steel, Constr. Build. Mater. 272 (2021), 121941, https://doi.org/10.1016/j.conbuildmat.2020.121941.
[44] 'UNE-EN 10002–1:2002, Metallic Materials - Tensile Testing - Part 1: Method of Test at Ambient Temperature'. AENOR.
[45] P. Larrinaga, D. García, L. Garmendia, J. Díez, and J.-T. San-José, 'Experimental Study on Flexural Behaviour of Low Strength/Quality Concrete Beams Strengthened with Textile Reinforced Mortar', presented at the 13th Structural Faults & Repair International Conference, Edinburgh, 2010.
[46] H. Cuypers, J. Wastiels, Stochastic matrix-cracking model for textile reinforced cementitious composites under tensile loading, Mater. Struct. Constr. 39 (2006) 777–786, https://doi.org/10.1617/s11527-005-9053-0.
[47] P. Larrinaga, 'Flexural Strengthening of Low-Grade Concrete Through the Use of New Cement-Based Composite Materials', Doctoral Thesis, University of the Basque Country (UPV/EHU), 2011.
[48] T. Silva de Carvalho, Reforço à Flexão de Vigas de Betão Armado com Compósitos de CFRP, Master Thesis (2010).
[49] 'Eurocode 2: Design of concrete structures Part 1: Common rules for building and civil engineering structures. prEN 1992–1′. CEN (Comité Européen de Normalisation). Eureopean Committee for Standardisation, Central Secretariat, Brussels, 2004.
[50] M. Malena, G. de Felice, Debonding of composites on a curved masonry substrate: Experimental results and analytical formulation, Compos. Struct. 112 (2014) 194–206, https://doi.org/10.1016/j.compstruct.2014.02.004.
[51] R.M. Richard, B.J. Abbot, Versatile Elastic-Plastic Stress-Strain Formula, in: J. Eng. Mech. ASCE 101, 4, 1975, pp. 511–515.
[52] C. Chastre, M.A.G. Silva, Monotonic axial behavior and modelling of RC circular columns confined with CFRP, Eng. Struct. vol. 32 (8) (. 2010) 2268–2277, https://doi.org/10.1016/j.engstruct.2010.04.001.
[53] R. Park, T. Paulay, Reinforced Concrete Structures, John Wiley & Sons, Inc, 1975.
[54] J.B. Mander, M.J.N. Priestley, R. Park, 'Seismic design of bridge piers, Research Report 84-2′, Department of Civil Engineering, University of Canterbury, Christchurch (1983).
[55] A. Esmaeily, Seismic behavior of bridge columns subjected to various loading patterns, PEER (2002) 321. Jan. 2002.
[56] P. Jiménez Montoya, A. García Meseguer, and F. Morán, Hormigón Armado. 14a Edición Basada en la EHE. 2000.
[57] 'EHE-08, Instrucción para el Proyecto y Ejecución de Obras de Hormigón en Masa y Armado.', Bol. . Estado BOE 203 (2008) 23701–23717.
[58] D.E. Branson, Deformation of Concrete Structures. 1971.
[59] U. Häußler-Combe, J. Hartig, Bond and failure mechanisms of textile reinforced concrete (TRC) under uniaxial tensile loading, Cem. Concr. Compos. 29 (4) (2007) 279–289, https://doi.org/10.1016/j.cemconcomp.2006.12.012.
[60] F. Jesse, , 'Tragverhalten von filamentgarnen in zementgebundener matrix (load bearing behaviour of filament yarns embedded in cementious matrix)' (Technische Universität, Dresden, Germany), Dr. Thesis, Fac. Civ. Eng. (2005) (Technische Universität, Dresden, Germany).
[61] J. Aveston, A. Kelly, Theory of multiple fracture of fibrous composites, J. Mater. Sci. 8 (3) (1973) 352–362, https://doi.org/10.1007/BF00550155.